Electronic Supplementary Information

Colloidal Nanocrystal Superlattices as Phononic Crystals: Plane Wave Expansion Modeling of Phonon Band Structure

Seid M. Sadat[1] and Robert Y. Wang[1*]

[1]*School for Engineering of Matter, Transport & Energy, Arizona State University, Tempe, Arizona 85287*

E-mail: rywang@asu.edu

Plane Wave Expansion Methodology

To determine the phonon band structure using the plane wave expansion method, we begin with the 3-dimensional elastic wave equation in terms of Lamé coefficients for a locally isotropic medium:[1-3]

$$\frac{\partial^2 u^i}{\partial t^2} = \frac{1}{\rho}\left[\frac{\partial}{\partial x_i}\left(\lambda\frac{\partial u^l}{\partial x_l}\right) + \frac{\partial}{\partial x_l}\left(\mu\left[\frac{\partial u^i}{\partial x_l} + \frac{\partial u^l}{\partial x_i}\right]\right)\right], i, l = 1,2,3 \quad (1)$$

where t is time, i and l are indices (1, 2, or 3), and u^i , u^l, x_i and x_l are the Cartesian components of the displacement vector, $\boldsymbol{u}(\boldsymbol{r})$, and position vector, $\boldsymbol{r}$, respectively. The spatially varying density, first Lamé coefficient, and second Lamé coefficient are represented by $\rho(\boldsymbol{r})$, $\lambda(\boldsymbol{r})$, and $\mu(\boldsymbol{r})$, respectively. Since a phononic crystal is periodic, any given local material property, f(**r**), is also periodic with respect to all lattice vectors, $\boldsymbol{R}$.

$$f(\boldsymbol{r} + \boldsymbol{R}) = f(\boldsymbol{r}) \quad (2a)$$

$$\boldsymbol{R} = n_1\boldsymbol{a_1} + n_2\boldsymbol{a_2} + n_3\boldsymbol{a_3} \quad (2b)$$

where *f(**r**)* is representative of $\rho(\boldsymbol{r})$, $\lambda(\boldsymbol{r})$, or $\mu(\boldsymbol{r})$ and n_i is an integer. Since this paper focuses on face-centered cubic systems, we use the following lattice vectors:

$$\boldsymbol{a_1} = \frac{a}{2}(\hat{x} + \hat{z}) \quad (3a)$$

$$\boldsymbol{a_2} = \frac{a}{2}(\hat{x} + \hat{y}) \quad (3b)$$

$$\boldsymbol{a_3} = \frac{a}{2}(\hat{y} + \hat{z}) \quad (3c)$$

where a represents the lattice constant of the conventional face-centered cubic lattice. We construct a triclinic primitive unit cell with 8 spheres at the corners using these three vectors (Figure S1b). Since $f(\boldsymbol{r})$ is a periodic function in space, it can be expanded in a 3-D Fourier series exploiting unit cell vectors and reciprocal lattice vectors (RLVs):

$$f(\boldsymbol{r}) = \sum_G f_G e^{jG.\boldsymbol{r}} \quad (4)$$

where

$$\boldsymbol{G} = m_1\boldsymbol{b_1} + m_2\boldsymbol{b_2} + m_3\boldsymbol{b_3} \quad (5)$$

$$\boldsymbol{b_1} = 2\pi\frac{\boldsymbol{a_2}\times\boldsymbol{a_3}}{\boldsymbol{a_1}.(\boldsymbol{a_2}\times\boldsymbol{a_3})}\ ,\ \boldsymbol{b_1} = \frac{2\pi}{a}(\hat{k}_x - \hat{k}_y + \hat{k}_z) \quad (6a)$$

$$\boldsymbol{b_2} = 2\pi\frac{\boldsymbol{a_3}\times\boldsymbol{a_1}}{\boldsymbol{a_2}.(\boldsymbol{a_3}\times\boldsymbol{a_1})}\ ,\ \boldsymbol{b_2} = \frac{2\pi}{a}(\hat{k}_x + \hat{k}_y - \hat{k}_z) \quad (6b)$$

$$\boldsymbol{b_3} = 2\pi \frac{\boldsymbol{a_1}\times\boldsymbol{a_2}}{\boldsymbol{a_3}.(\boldsymbol{a_1}\times\boldsymbol{a_2})}\ ,\ \boldsymbol{b_3} = \frac{2\pi}{a}(\hat{k}_y - \hat{k}_x + \hat{k}_z) \tag{6c}$$

where **G** is a reciprocal lattice vector, m_i is an integer, and $\boldsymbol{b}_i$ are reciprocal lattice unit vectors. Since the local material properties are periodic functions of the position vector, the Floquet-Bloch theorem[4] tells us that the eigensolutions of the wave equation are modulated sinusoids of the form:

$$u(r) = u_{\boldsymbol{k}}(r)e^{j(\boldsymbol{k}\cdot\boldsymbol{r})} \tag{7}$$

where

$$u_{\boldsymbol{k}}(\boldsymbol{r}) = u_{\boldsymbol{k}}\left(\boldsymbol{r} + \textstyle\sum_{i=1,2,3} n_i \boldsymbol{a_i}\right) \tag{8}$$

The displacements, $u_{\boldsymbol{k}}$, are also periodic and can be expanded in a 3-D Fourier series:

$$u(r) = \left(\textstyle\sum_{\boldsymbol{G}} u_{\boldsymbol{k}+\boldsymbol{G}}\right)e^{j\boldsymbol{k}\cdot\boldsymbol{r}} = \textstyle\sum_{\boldsymbol{G}} u_{\boldsymbol{k}+\boldsymbol{G}}\, e^{j(\boldsymbol{k}+\boldsymbol{G})\cdot\boldsymbol{r}} \tag{9}$$

We consider plane wave solutions of the form shown in Equation 10, where *j* is the imaginary unit and ω is angular frequency:

$$u = e^{j(\boldsymbol{k}\cdot\boldsymbol{r}-\omega t)} \tag{10}$$

By substituting Equations 4, 9, and 10 into Equation 1, we can arrive at the following equation:

$$\begin{aligned}\omega^2 u^i_{\boldsymbol{k_0}+\boldsymbol{G}} = \sum_{G'}\Bigg[\sum_{l,G} \rho^{-1}_{\boldsymbol{G}-\boldsymbol{G''}}\,[\lambda_{\boldsymbol{G''}-\boldsymbol{G'}}(\boldsymbol{k_0}+\boldsymbol{G'})_l(\boldsymbol{k_0}+\boldsymbol{G''})_i \\ + \mu_{\boldsymbol{G''}-\boldsymbol{G'}}(\boldsymbol{k_0}+\boldsymbol{G'})_i(\boldsymbol{k_0}+\boldsymbol{G''})_l]u^l_{\boldsymbol{k_0}+\boldsymbol{G'}} \\ + \sum_{\boldsymbol{G''}}\left(\rho^{-1}_{\boldsymbol{G}-\boldsymbol{G''}}\,\mu_{\boldsymbol{G''}-\boldsymbol{G'}}\sum_n (\boldsymbol{k_0}+\boldsymbol{G'})_n(\boldsymbol{k_0}+\boldsymbol{G''})_n\right)u^i_{\boldsymbol{k_0}+\boldsymbol{G'}}\Bigg]\end{aligned} \tag{11}$$

where $\boldsymbol{k_o}$ is a wave vector, $\boldsymbol{G}, \boldsymbol{G'}$ and $\boldsymbol{G''}$ are reciprocal lattice vectors, and *i*, *l*, and *n* are indices that vary between 1, 2, and 3. Equation 11 can be rewritten in an eigenvector-eigenvalue matrix form, $AU = U\Lambda$, where U is the eigenvector matrix, Λ is eigenvalue matrix, and A is a matrix of coefficients.

$$A_{G_i,G'_l} = \textstyle\sum_{G''}\rho^{-1}_{\boldsymbol{G_i}-\boldsymbol{G''}}\left[\begin{array}{c}\lambda_{\boldsymbol{G''}-\boldsymbol{G'_n}}\begin{bmatrix}(\boldsymbol{k_0}+\boldsymbol{G''})_x(\boldsymbol{k_0}+\boldsymbol{G'_l})_x & (\boldsymbol{k_0}+\boldsymbol{G''})_x(\boldsymbol{k_0}+\boldsymbol{G'_l})_y & (\boldsymbol{k_0}+\boldsymbol{G''})_x(\boldsymbol{k_0}+\boldsymbol{G'_l})_z\\ (\boldsymbol{k_0}+\boldsymbol{G''})_y(\boldsymbol{k_0}+\boldsymbol{G'_l})_x & (\boldsymbol{k_0}+\boldsymbol{G''})_y(\boldsymbol{k_0}+\boldsymbol{G'_l})_y & (\boldsymbol{k_0}+\boldsymbol{G''})_y(\boldsymbol{k_0}+\boldsymbol{G'_l})_z\\ (\boldsymbol{k_0}+\boldsymbol{G''})_z(\boldsymbol{k_0}+\boldsymbol{G'_l})_x & (\boldsymbol{k_0}+\boldsymbol{G''})_z(\boldsymbol{k_0}+\boldsymbol{G'_l})_y & (\boldsymbol{k_0}+\boldsymbol{G''})_z(\boldsymbol{k_0}+\boldsymbol{G'_l})_z\end{bmatrix}\\ +\mu_{\boldsymbol{G''}-\boldsymbol{G'_n}}\begin{bmatrix}(\boldsymbol{k_0}+\boldsymbol{G'_l})_x(\boldsymbol{k_0}+\boldsymbol{G''})_x & (\boldsymbol{k_0}+\boldsymbol{G'_l})_x(\boldsymbol{k_0}+\boldsymbol{G''})_y & (\boldsymbol{k_0}+\boldsymbol{G'_l})_x(\boldsymbol{k_0}+\boldsymbol{G''})_z\\ (\boldsymbol{k_0}+\boldsymbol{G'_l})_y(\boldsymbol{k_0}+\boldsymbol{G''})_x & (\boldsymbol{k_0}+\boldsymbol{G'_l})_y(\boldsymbol{k_0}+\boldsymbol{G''})_y & (\boldsymbol{k_0}+\boldsymbol{G'_l})_y(\boldsymbol{k_0}+\boldsymbol{G''})_z\\ (\boldsymbol{k_0}+\boldsymbol{G'_l})_z(\boldsymbol{k_0}+\boldsymbol{G''})_x & (\boldsymbol{k_0}+\boldsymbol{G'_l})_z(\boldsymbol{k_0}+\boldsymbol{G''})_y & (\boldsymbol{k_0}+\boldsymbol{G'_l})_z(\boldsymbol{k_0}+\boldsymbol{G''})_z\end{bmatrix}\\ +\mu_{\boldsymbol{G''}-\boldsymbol{G'_l}}(\textstyle\sum_n(\boldsymbol{k_0}+\boldsymbol{G'_l})_n(\boldsymbol{k_0}+\boldsymbol{G''})_n)I_3\end{array}\right] \tag{12a}$$

$$A = \left[A_{\boldsymbol{G_i},\boldsymbol{G'_l}}\right]_{i,l\in 1\ldots M} \tag{12b}$$

$$U = \begin{bmatrix} u^{1,x}_{\mathbf{k_0}-\mathbf{G_1}} & & u^{3M,x}_{\mathbf{k_0}-\mathbf{G_1}} \\ u^{1,y}_{\mathbf{k_0}-\mathbf{G_1}} & \cdots & u^{3M,y}_{\mathbf{k_0}-\mathbf{G_1}} \\ u^{1,z}_{\mathbf{k_0}-\mathbf{G_1}} & & u^{3M,z}_{\mathbf{k_0}-\mathbf{G_1}} \\ \vdots & & \vdots \\ u^{1,x}_{\mathbf{k_0}-\mathbf{G_M}} & & u^{3M,x}_{\mathbf{k_0}-\mathbf{G_M}} \\ u^{1,y}_{\mathbf{k_0}-\mathbf{G_M}} & \cdots & u^{3M,y}_{\mathbf{k_0}-\mathbf{G_M}} \\ u^{1,z}_{\mathbf{k_0}-\mathbf{G_M}} & & u^{3M,z}_{\mathbf{k_0}-\mathbf{G_M}} \end{bmatrix} \tag{12c}$$

$$\Lambda = \begin{bmatrix} \omega_1^2 & & 0 & & 0 \\ & \ddots & 0 & 0 & \\ 0 & 0 & \ddots & 0 & 0 \\ & 0 & 0 & \ddots & \\ 0 & & 0 & & \omega_{3M}^2 \end{bmatrix} \tag{12d}$$

where $(\boldsymbol{k_0} + \boldsymbol{G})_i$ refers to the component of $(\boldsymbol{k_0} + \boldsymbol{G})$ in direction *i* and *M* represents the total number of Fourier coefficients utilized in each of the three dimensions. Solving the above matrix equation yields the eigenvalues, ω, of the eigenvector, $\boldsymbol{k_o}$. Varying $\boldsymbol{k_o}$ throughout the Brillouin zone then allows the phonon band diagram to be mapped out.

In practice, a finite number of RLVs must be chosen when doing the Fourier expansion shown in Equation 4. To do this we use a centered numerical Fourier transform with 301 terms (i.e., -150,… , 0, …. 150) for each of the three dimensions. For our numerical Fourier transform we utilized the FFTW package.[5] However, using all 301 term in Equation 12 would yield intractably large matrices. For computational purposes, we utilize a centered *2m + 1* subset of these terms (i.e. *-m*, *-(m-1)*, …, 0, …, *m-1*, *m*). The total number of Fourier coefficients utilized in each dimension is then *M = 2m + 1*. For the calculations in our paper, we use *m* = 8 (i.e. *M* = 17) in each of the three dimensions, which leads to a total number of 729 RLVs for our phononic band diagram calculations. We conducted a numerical convergence test by systematically increasing the value of *m* in a model phononic crystal system. We found that increasing *m* beyond 8 led to very small ~1% changes in the frequencies of the phonon bands (Figure S2). We also confirmed the numerical accuracy of our code by benchmarking it against PWE results in the literature (Figure S2).[1]

For the purposes of mapping out the phonon band diagram, we choose $\boldsymbol{k_0}$ values along the edges of the irreducible first Brillouin zone (Figure S1C). Table 1 shows the Cartesian coordinates of the symmetry points of the Brillouin zone. We moved $\boldsymbol{k_0}$ along the path of X-L-U-Γ-X-W-K and chose 20 points along each segment. We utilized the parallel computing library, Message Passing Interface (MPI),[6] to expedite computational time. We also structured our code to separate our chosen $\boldsymbol{k_0}$ points among multiple cores. This allows the eigenfrequencies of multiple $\boldsymbol{k_0}$ points to be computed in parallel, and leads to a decrease in computational time by a factor of *1/n*, where *n* is the number of cores.

Phononic Band Gap Characteristics as a Function of Nanocrystal Core Volume Fraction

The main text of this paper presents the phononic band gap characteristics as a function of nanocrystal core diameter, *d*, and interparticle distance, *L*. Since the interparticle distance is determined by the organic ligand length, varying *d* and *L* is equivalent to varying the nanocrystal core volume fraction. The

relationship between nanocrystal core volume fraction is given by the equation below and is also illustrated in Figure S3.

$$Nanocrystal\ Core\ Volume\ Fraction = \frac{\pi}{3\sqrt{2}}\left(\frac{d}{d+L}\right)^3 \quad (13)$$

In some instances, it may be more convenient to see the phononic band gap characteristics as a function of nanocrystal core volume fraction instead of nanocrystal diameter. This data is shown in Figures S4 and S5 below (which are equivalent to Figures 4 and 5 in the main text).

The Effect of Poisson's Ratio on the Phononic Band Gap

We calculated the impact of the nanocrystal core Poisson's ratio, $\nu_{NC\ Core}$, and the ligand matrix Poisson's ratio, ν_{ligand}, on the phononic band gap center frequency and width. We found that varying Poisson's ratio from 0.1 – 0.4 has only a minor effect on the band gap characteristics (Figure S6).

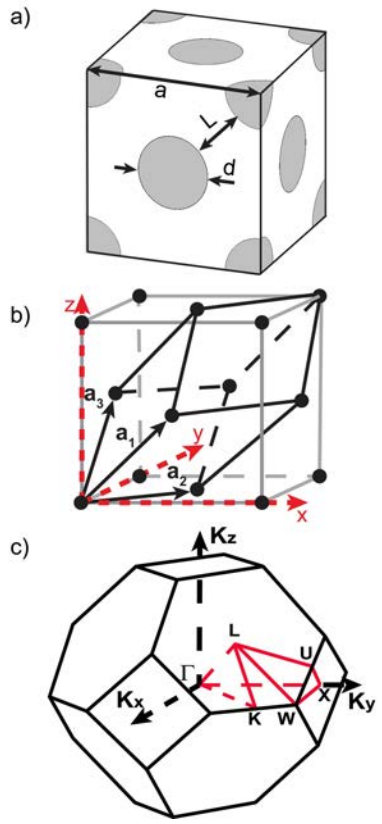

Figure S1. (a) Schematic of the conventional unit cell for a face-centered cubic lattice with relevant geometrical parameters labeled: interparticle distance, *L*, lattice constant, *a,* and nanocrystal core diameter, *d*. (b) Schematic of a primitive unit cell (black lines) for a face-centered cubic lattice and corresponding primitive cell lattice vectors, $\boldsymbol{a_1}$, $\boldsymbol{a_2}$, and $\boldsymbol{a_3}$. (c) Schematic of the first Brillouin zone (black lines) and the irreducible region of the first Brillouin zone (red lines).

Point	Cartesian Coordinates, $[\hat{k}_x, \hat{k}_y, \hat{k}_z]$
Γ	$[0,0,0]$
X	$[0, \frac{2\pi}{a}, 0]$
L	$[\frac{\pi}{a}, \frac{\pi}{a}, \frac{\pi}{a}]$
W	$[\frac{\pi}{a}, \frac{2\pi}{a}, 0]$
U	$[\frac{\pi}{2a}, \frac{2\pi}{a}, \frac{\pi}{2a}]$
K	$[\frac{3\pi}{2a}, \frac{3\pi}{2a}, 0]$

Table 1. The Cartesian coordinates of the key symmetry points in the Brillouin zone of a face-centered cubic lattice.

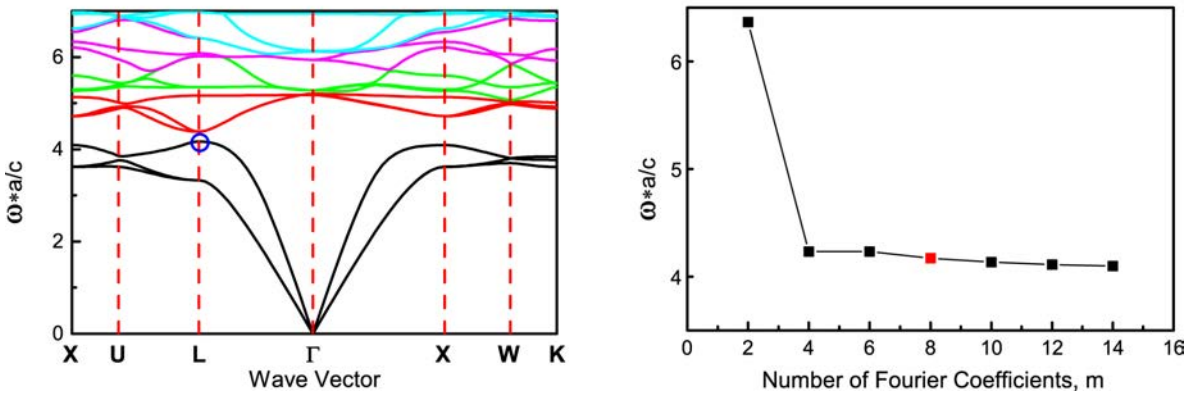

Figure S2. (a) The phonon band diagram of Au spheres in a Si matrix for a face-centered cubic lattice. Note that we have used normalized frequency ω^*a/c (c is the transverse speed of sound in the matrix material) in this band diagram. This band diagram agrees with the PWE results in Reference 1 and confirms the numerical accuracy of our code. (b) The normalized frequency of the 3rd band at symmetry point L as a function of the parameter, m. Increasing m beyond the value used in this paper (m = 8) leads to negligible changes in phonon frequency. For clarity we have used a blue circle in part (a) to mark the frequency location of the 3rd band at symmetry point L.

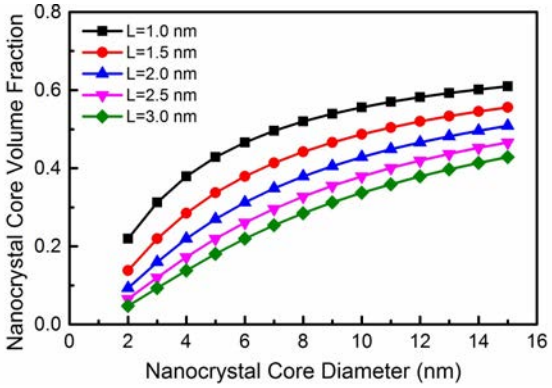

Figure S3. The nanocrystal core volume fraction in a nanocrystal superlattice as a function of nanocrystal core diameter, d, and interparticle distance, L.

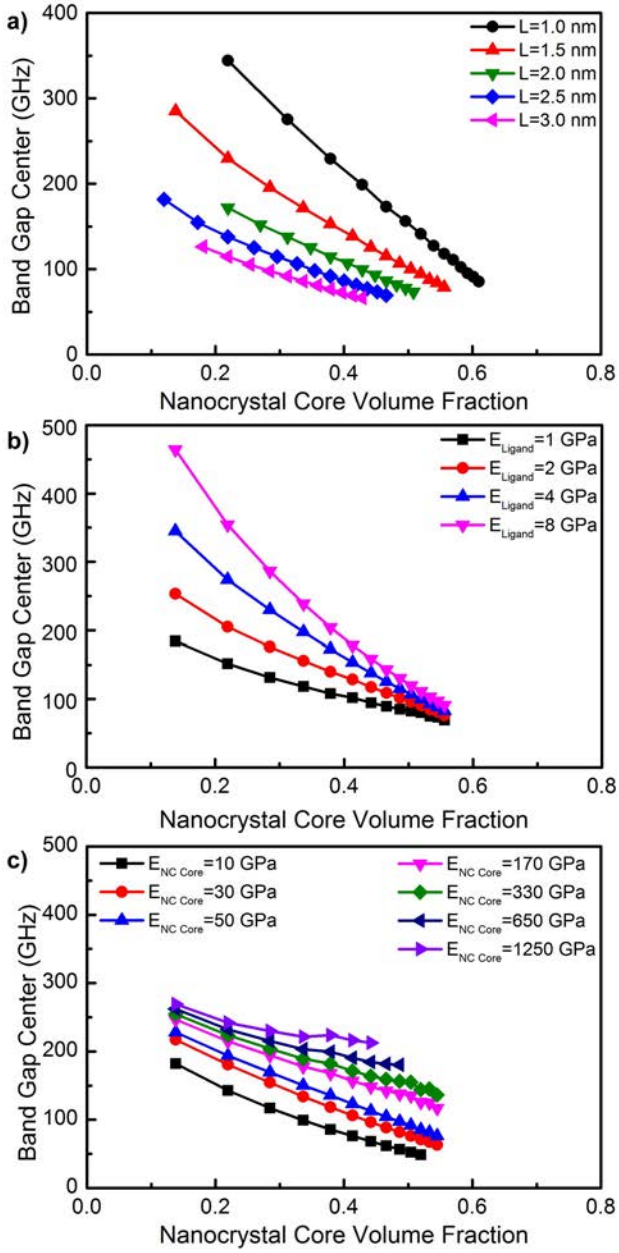

Figure S4. The effect of nanocrystal core volume fraction on the center frequency of the phononic band gap for: (a) varying interparticle distance, L; (b) varying elastic modulus of the ligand matrix, E_{ligand}; and (c) varying elastic modulus of the nanocrystal core, $E_{NC\ Core}$. Unless otherwise specified, L, E_{ligand}, and $E_{NC\ Core}$ are fixed at 1.5 nm, 2.6 GPa, and 54 GPa, respectively.

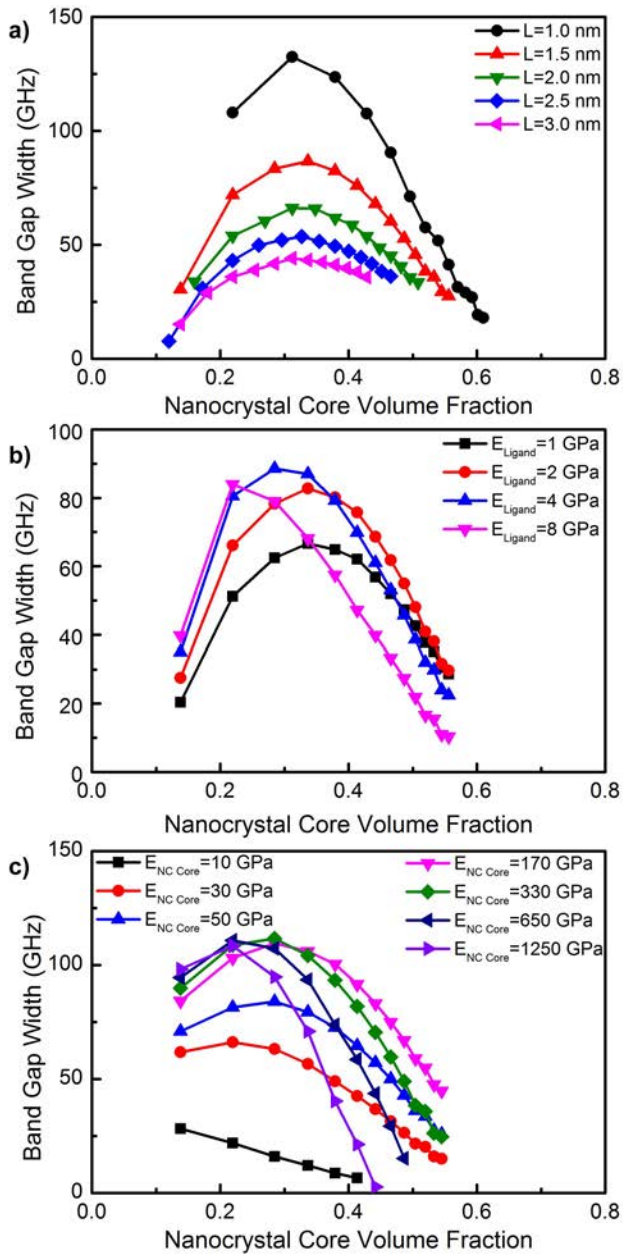

Figure S5. The effect of nanocrystal core volume fraction on the phononic band gap width for: (a) varying interparticle distance, L; (b) varying elastic modulus of the ligand matrix, E_{ligand}; and (c) varying elastic modulus of the nanocrystal core, $E_{NC\ Core}$. Unless otherwise specified, L, E_{ligand}, and $E_{NC\ Core}$ are fixed at 1.5 nm, 2.6 GPa, and 54 GPa, respectively.

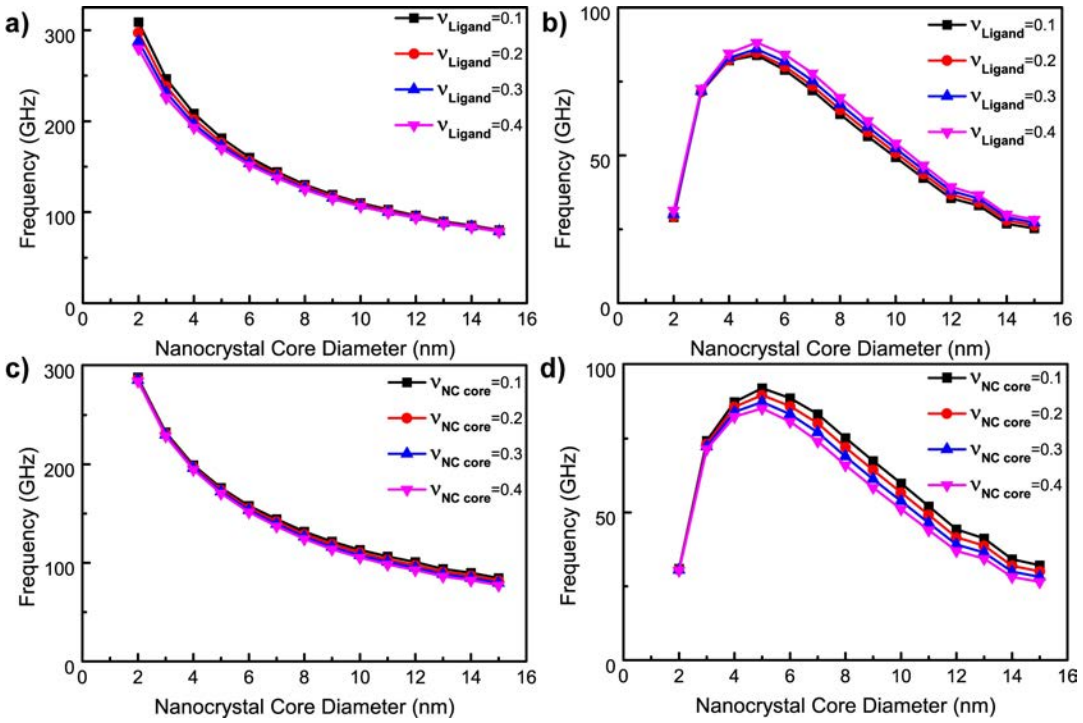

Figure S6. The effect of ligand Poisson ratio, v_{ligand}, on the (a) phononic band gap center frequency and (b) phononic band gap width; and the effect of nanocrystal core Poisson ratio, $v_{NC\ Core}$, on the (a) phononic band gap center frequency and (b) phononic band gap width. In parts (a – d), the following parameters are used: L = 1.5 nm, E_{ligand} = 2.6 GPa, and $E_{NC\ Core}$ = 54 GPa.

References

1. E. N. Economou and M. Sigalas, *The Journal of the Acoustical Society of America*, 1994, **95**, 1734-1740.
2. H. Ibach, H. Lüth, L. Mihaly and D. Mandrus, *American Journal of Physics*, 1992, **60**, 1053-1054.
3. D. W. Wright, PhD Thesis, University of Toronto, 2010.
4. D. Sjöberg, C. Engström, G. Kristensson, D. J. Wall and N. Wellander, *Multiscale Modeling & Simulation*, 2005, **4**, 149-171.
5. FFTW, (http://www.fftw.org/).
6. Open MPI: Open Source High Performance Computing, (https://www.open-mpi.org/).